APL Materials

Identification of Li_{Ni} and V_{Ni} acceptor levels in doped nickel oxide

Cite as: APL Mater. **8**, 121106 (2020); https://doi.org/10.1063/5.0032102
Submitted: 06 October 2020 . Accepted: 30 November 2020 . Published Online: 24 December 2020

Robert Karsthof, Holger von Wenckstern, Vegard Skiftestad Olsen, and Marius Grundmann

COLLECTIONS

F This paper was selected as Featured

ARTICLES YOU MAY BE INTERESTED IN

A new era in ferroelectrics
APL Materials **8**, 120902 (2020); https://doi.org/10.1063/5.0034914

Electrically driven transient and permanent phase transformations in highly strained epitaxial $BiFeO_3$ thin films
APL Materials **8**, 101110 (2020); https://doi.org/10.1063/5.0025673

MXene improves the stability and electrochemical performance of electropolymerized PEDOT films
APL Materials **8**, 121105 (2020); https://doi.org/10.1063/5.0023187

© 2020 Author(s).

Identification of Li_{Ni} and V_{Ni} acceptor levels in doped nickel oxide

Cite as: APL Mater. 8, 121106 (2020); doi: 10.1063/5.0032102
Submitted: 6 October 2020 • Accepted: 30 November 2020 •
Published Online: 24 December 2020

View Online

Export Citation

CrossMark

Robert Karsthof,[1,a] Holger von Wenckstern,[1] Vegard Skiftestad Olsen,[2] and Marius Grundmann[1]

AFFILIATIONS

[1] Universität Leipzig, Felix-Bloch-Institut für Festkörperphysik, Linnéstr. 5, 04103 Leipzig, Germany
[2] Department of Physics, Universitetet i Oslo, Gaustadalléen 23A, 0373 Oslo, Norway

[a] **Author to whom correspondence should be addressed:** r.m.karsthof@smn.uio.no. **Current Address:** Center for Materials Science and Nanotechnology, Universitetet i Oslo, Gaustadalléen 23A, 0373 Oslo, Norway.

ABSTRACT

Nickel oxide, in particular in its doped, semiconducting form, is an important component of several optoelectronic devices. Doped NiO is commonly achieved either by incorporation of lithium, which readily occupies Ni sites substitutionally, producing the Li_{Ni} acceptor, or by supplying reactive oxygen species during NiO film deposition, which leads to the formation of Ni vacancies (V_{Ni}). However, the energetic position of these acceptors in the NiO bandgap has not been experimentally determined until today. In this work, we close this knowledge gap by studying rectifying $n^{++}p$ heterojunctions consisting of NiO thin films grown on top of fluorine-doped tin oxide. These structures show sufficient rectification to perform electric characterization by defect spectroscopic techniques, specifically capacitance–voltage and thermal admittance spectroscopy. Using these methods, the (0/−) charge transition levels are determined to be 190 meV and 409 meV above the valence band edge for the Li_{Ni} and the V_{Ni} acceptor, respectively.

© 2020 Author(s). All article content, except where otherwise noted, is licensed under a Creative Commons Attribution (CC BY) license (http://creativecommons.org/licenses/by/4.0/). https://doi.org/10.1063/5.0032102

I. INTRODUCTION

Nickel oxide is one of the rare examples of a *p*-type semiconducting metal oxide. Because of its high bandgap of 3.8 eV, it is transparent in the visible spectral range, making it interesting for a variety of optoelectronic bipolar devices, such as organic[1–3] and perovskite solar cells,[4] light-emitting diodes,[5,6] electrochromic devices,[7–10] and resistive-switching elements.[11,12] For many of these applications, doping is a key element in obtaining functional layers and devices because pure, stoichiometric NiO is known to be an insulator. The knowledge of the energetic positions of acceptor states with respect to the valence band edge is important when it comes to tailoring NiO properties to the requirements of the respective device. For example, heavy doping may lead to Fermi level pinning, which in turn impacts the band alignment in heterostructures. Acceptor doping of NiO is typically achieved by either incorporating Li into the NiO lattice, which substitutes for Ni and contributes a single hole to the electronic system, or by growing the sample under an oversupply of oxygen, which renders the specimen Ni-deficient, producing nickel vacancy (V_{Ni}) double acceptors. In both cases, the holes are rather tightly bound to the acceptors, and it has been shown that the carriers are localized mainly in the O 2*p* states of the immediate ionic neighborhood.[13,14] Even though there exist some (mostly theoretical) studies that estimate the positions of the charge transition levels (CTLs) associated with these acceptors (see Table I), no experimental verification of these estimates has been published to date. In our view, this is a result of a lack of rectifying NiO-based structures, i.e., Schottky or heterodiodes, with a depletion layer located within the NiO layer that enables the use of conventional defect spectroscopical techniques, such as thermal admittance spectroscopy (TAS). This is mainly due to the low electron affinity of NiO of only around 1.5 eV,[15] limiting the choice of materials with even lower work functions to achieve hole depletion.

In this work, we show that n^{++}-SnO_2:F/*p*-NiO heterocontacts possess the desired properties in that they lead to a considerable depletion layer width of 25 nm–35 nm at 0 V bias, and a band bending of roughly 0.5 V, making capacitance–voltage measurements and thermal admittance spectroscopy and the determination of the acceptor charge transition levels possible. At the same time, the current study can be considered a test case for these techniques

© Author(s) 2020

TABLE I. Literature values for the expected charge transition levels of the Li cation-substitutional and the Ni vacancy acceptors. All values in meV with respect to the valence band maximum.

Li_{Ni}	V_{Ni}		
(0/−)	(0/−)	(−/2−)	Method/references
250	480	720	Theor.[16]
153	515		Theor.[17]
	260	370	Theor.[18]
	−30	160	Theor.[19]
400	600	800	Theor.[20]
	400	600	Theor.[21]
190	409		Exp. (this work)

regarding their ability to reliably probe trap levels in materials with extremely low hole mobilities.

II. EXPERIMENTAL METHODS

NiO films were deposited on top of commercial SnO_2:F (FTO)-coated glass substrates purchased from Calyxo GmbH, Germany ($\sigma_{FTO} = 2.5 \times 10^3$ S cm^{-1} and $n_{FTO,\,Hall} = 5.5 \times 10^{20}$ cm^{-3}). NiO growth was performed by pulsed laser deposition (PLD) using a KrF excimer laser (wavelength 248 nm and pulse energy 650 mJ) ablating either ceramic targets consisting of either pure NiO (purity 99.998%) or 0.5 at. % Li-doped NiO. For the Li-doped target, Li_2CO_3 and NiO powders were mixed in a Li:Ni 1:200 molarity ratio. Both targets were then fabricated by ball milling of the powders, pressing into disks, and subsequent sintering in air at 1350 °C for 24 h. The film growth was done either at room temperature (no intentional substrate heating) or at a substrate temperature of 300 °C. The partial pressure of the background oxygen gas was chosen between 0.02 mbar for Li-doping and 0.1 mbar for introducing an excess of oxygen during growth. The thicknesses of the NiO films were between 100 nm and 290 nm. For uniform current flow, the NiO layers were capped by a 20 nm thick Pt layer deposited by DC magnetron sputtering. In addition to PLD, NiO growth was also achieved by reactive DC magnetron sputtering from a metallic Ni target at room temperature in an Ar/O_2 atmosphere (p_{O2} = 0.028 mbar, total pressure 0.04 mbar, and flow ratio Ar/O_2 5:8). The sputtered NiO layers were then capped with Pt in the same way as the PLD NiO films. As shown in Ref. 22, Pt/NiO contacts do not induce a depletion region in NiO and can be considered ohmic for small voltages around 0 V.

For the room temperature-grown NiO, the NiO/Pt top contact structure was patterned into pillars with circular cross sections (diameter between 250 μm and 800 μm) by subsequent deposition of both films through a previously structured photoresist mask. For the high temperature-grown NiO film, only the Pt contacts were patterned (by the same method).

Current–voltage characterization was carried out with an AGILENT 4155C semiconductor parameter analyzer connected to a Süss wafer prober system using tungsten needles. These measurements were used to select individual contacts for the defect spectroscopy measurements. The samples were then mounted onto transistor sockets, and the selected pillars were bonded with Au wires and conductive silver epoxy resin. Defect spectroscopic measurements were carried out in a He flow cryostat (20 K < T_{meas} < 360 K). For the C–V and TAS measurements, an AGILENT 4294A was used (measurement frequency between 40 Hz and 1 MHz and AC probing voltage 50 mV). For TAS, no additional DC bias was applied.

III. RESULTS

Figure 1 shows typical current density–voltage (j–V) characteristics measured on the NiO/FTO heterostructures. The rectification ratio $S_R = |j(1V)/j(-1V)|$ takes on values between 3 orders of magnitude for the magnetron-sputtered NiO and 1.3 orders of magnitude for the high temperature-grown, oxygen excess-doped NiO. Based on the general diode equation,

$$j = j_s\left[\exp\left(\frac{eV}{n_{id}k_BT}\right) - 1\right], \quad (1)$$

with j_s being the saturation current density and n_{id} ideality factor of the diode, e elementary charge, k_B Boltzmann's constant, and

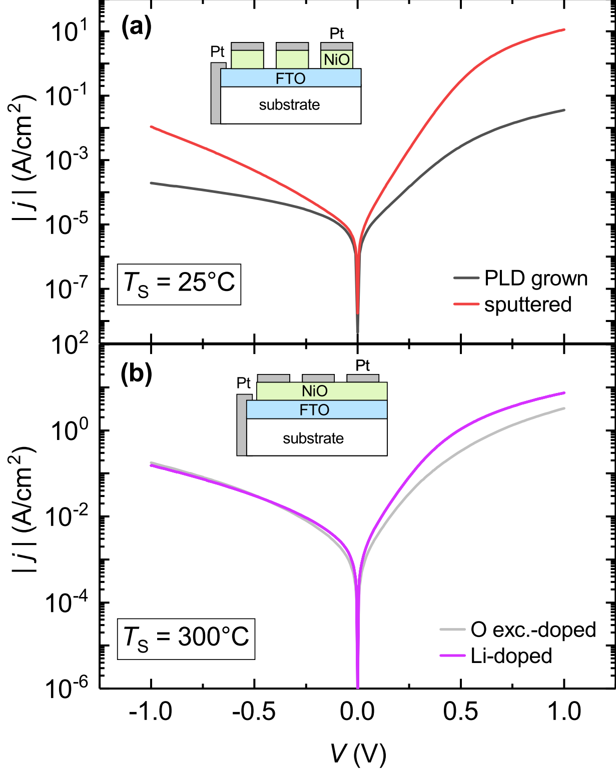

FIG. 1. Current density–voltage relations of different NiO/FTO structures. (a) NiO grown at room temperature, using PLD and magnetron sputtering, and (b) NiO grown at a substrate temperature of about 300 °C, using oxygen excess or Li incorporation for doping. The insets show cross-sectional schematics of the sample structure.

© Author(s) 2020

$T = 300$ K measurement temperature, diode ideality factors between 1.7 for magnetron sputtered NiO and 2.8 for room temperature PLD-grown NiO can be derived. In the case of high temperature-grown NiO, a monoexponential increase of the current density cannot be discerned. For an ideal one-sided heterojunction where one junction partner is considerably higher doped than the other, which is shown to be the case in the further course of this work, an ideality factor close to 1 is expected. The deviation of n_{id} from unity becomes comprehensible in the framework of the multicontact model developed by Johnson, Smith, and Yearian.[23] In that model, lateral variations within the contact area of certain diode properties, such as local built-in potential and electrical conductivity, can give rise to such observations. We infer that lateral inhomogeneities of the NiO layer doping are responsible for the increased values of n_{id}. In any case, it can be stated that NiO growth on top of FTO reliably leads to a depletion region in the NiO film, independent of the growth method, conditions, and patterning.

In Fig. 2, profiles of the net doping density N_{net} with varying space charge region (SCR) width w from all four NiO film types are displayed, as obtained by means of capacitance–voltage (C–V) measurements, using the following relations:

$$N_{net} = -\frac{2}{e\varepsilon_r\varepsilon_0 A^2}\left(\frac{d}{dV}C^{-2}\right)^{-1}, \tag{2}$$

$$w = \frac{\varepsilon_s\varepsilon_0 A}{C}, \tag{3}$$

where $\varepsilon_r\varepsilon_0 = 11.6\varepsilon_0$ is the NiO dielectric permittivity and A the cross-sectional area of the contact. The voltage range used was between −0.5 V and 0.1 V. The net doping ranges between some 10^{17} cm^{-3} for the Li-doped NiO and slightly above 10^{19} cm^{-3} for the sputtered NiO. The inset of Fig. 2 shows the frequency dependence of the capacitance for all four sample types. It becomes apparent that for the sputtered and the Li- and O excess-doped HT-grown films, a broad spectral region exists where C is a constant down to the lowest frequency measurable with our setup (40 Hz). Only for the film grown by PLD at room temperature, the frequency dependence exhibits a continuous decrease across the entire frequency range. Such a behavior is often characteristic of a broad distribution of electronic states participating in carrier displacement. Under AC electric fields at low frequencies, electronic charges are being exchanged periodically between states below and above the Fermi level. Increasing the frequency of the AC field leads to a progressive cutoff of higher-lying states, such that only states with energies closer to the Fermi level can participate. As a result, the dynamically determined capacitance is a decreasing function of the measurement frequency. For the Li- and O excess-doped as well as the sputtered NiO, the distribution of density of states appears to be rather narrow, as exemplified by the almost constant capacitance up to the MHz range. For the RT-PLD film, the dispersion is indicative of a broad distribution of electronic states, in accordance with the results from our earlier work.[22] The charge density profile for that sample, as shown in Fig. 2, must therefore be considered a lower boundary for the actual carrier concentration. For the other samples, the charge concentration is more reliable. It is worth noting that the charge carrier density of the Li-doped sample is more than two orders of magnitude lower than the Li content in the powder mixture used for PLD target preparation. This is likely due to a combination of preferential evaporation of Li during target sintering, stronger scattering of light Li-rich particles by background oxygen in the plasma plume during PLD, and easier desorption of Li as compared to NiO from the hot substrate during film growth. In addition, the incorporation efficiency of Li on Ni sites, where they act as the desired acceptors, is not necessarily unity, as shown in Ref. 24.

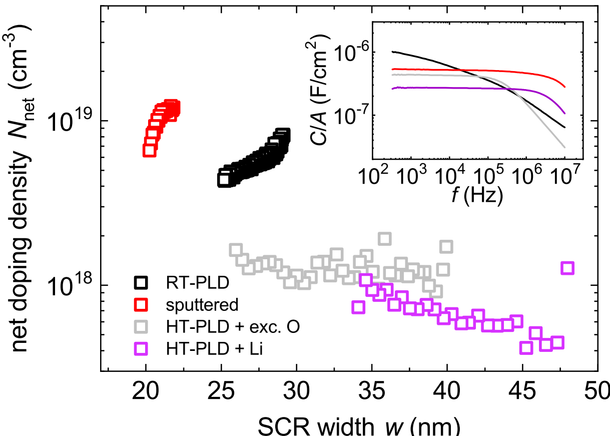

FIG. 2. Charge concentration profiles of NiO/FTO heterostructures with differently deposited NiO layers, as obtained from C–V measurements. Inset: frequency dependence of the capacitance per unit area at $V = 0$ V.

Another important point to be noticed from the data in Fig. 2 is the fact that doping with O excess achieves higher carrier concentrations in room temperature processes than for high-temperature growth. This is, again, in accordance with our earlier work[25] and also with the results from Gutiérrez *et al.*:[26] elevated temperatures cause the Ni vacancy acceptors brought into the film under non-equilibrium conditions to dissolve by the release of oxygen, thereby returning to a concentration that is closer to the thermodynamic equilibrium value. This process already occurs during growth and leads to NiO films grown at a higher temperature exhibiting a lower carrier concentration than the ones grown at room temperature, even though the same oxygen partial pressures were used. In the further course of this paper, we will focus on the high-temperature grown samples. This is, in part, due to higher stability of the defect population herein, but also because of a higher degree of disorder in the room temperature fabricated films, which makes a unique assignment of defect signatures difficult. The difference in disorder between low- and high-temperature grown NiO films had been demonstrated before by structural investigations by means of x-ray diffraction:[22] room temperature growth typically leads to polycrystalline films consisting of small crystallites (around 5 nm) when using PLD, and even x-ray amorphous films for sputtering. PLD growth at elevated temperatures of 300 °C promotes a polycrystalline structure with larger grains. A wide-angle 2θ-ω scan of a 0.5 at. % Li-doped NiO layer on top of FTO-coated glass substrates is shown in Fig. S1 of the supplementary material, exemplifying a slight preferential NiO growth along the [220] direction and suggesting a lower bound for the NiO crystallite size of approximately 85 nm.

© Author(s) 2020

Thermal admittance spectroscopy (TAS) measures the frequency and temperature dependence of the complex admittance $\underline{Y}$. A typical way of modeling admittance measurements of diodes is using an equivalent circuit consisting of a capacitor (capacitance C) and a parallel resistor (conductance G). In this case, $\underline{Y} = G + i\omega C$, with $\omega = 2\pi f$. The frequency dependence of both G and C is governed by the displacement of mobile charge carriers. For conventional band semiconductors, this consists of two contributions: free carriers at the edge of the space charge region are periodically moved back and forth within the (conduction or valence) band, while electronic defects with states within the semiconductor bandgap can be filled and emptied during one period of the AC voltage as long as their energy level crosses the Fermi energy within the SCR. Because the ionization and neutralization of defects are tied to the emission and capture of mobile carriers to and from a nearby band, the rate of this process is limited. At a certain critical frequency of the applied AC voltage, carrier emission will be too slow to follow, and the modulation of the defect's charge state will cease. This cutoff is visible in the spectra of both real and imaginary parts of $\underline{Y}$: a step appears in C (or equivalently, a peak in the derivative dC/dT), while the quantity G/ω exhibits a peak. The frequency ω_0 at which the cutoff appears is related to the emission rate e_p of the defect level and can be described by (in the case of a p-type semiconductor)

$$\omega_0 \approx 2e_p = 2\nu_0 \exp\left(-\frac{E_t}{k_B T}\right) = 2v_{th}\sigma_p N_V \exp\left(-\frac{E_t}{k_B T}\right) \propto T^2 \exp\left(-\frac{E_t}{k_B T}\right), \quad (4)$$

with ν_0 being the escape attempt frequency, E_t the distance of the trap level to the nearmost band, v_{th} the thermal velocity of the free carriers, σ_p the defect's capture cross section for holes, and N_V the effective density of states in the valence band.[27] Here, $v_{th} \propto T^{1/2}$ and $N_V \propto T^{3/2}$ are assumed. Equation (4) shows that carrier emission is thermally activated with an energy E_t. Therefore, the corresponding cutoff features in C and G/ω will also show a shift with the measurement temperature. An Arrhenius plot of e_p/T^2 then yields the depth E_t of the trap as well as its capture cross section σ_p. In Fig. 3(a), the capacitance C differentiated with respect to the temperature is shown for a selected diode on the Li-doped and O-excess NiO film as a function of temperature for a few measurement frequencies. A well-resolved peak appears for both samples, and apart from this one feature per sample type, no other peaks are observed within the accessible temperature range. Figure 3(b) displays the temperature dependence of the associated emission rates of the peaks, calculated based on Eq. (4), and a simple temperature activation becomes apparent. Three to four diodes were characterized per sample, and the data shown in Fig. 3 are representative of typical results. By fitting the data based on Eq. (4), and using values for the thermal hole velocity of the order of $v_{p,th} \approx 10^7$ cm s^{-1} and $N_V \approx 10^{19}$ cm^{-3}, trap energies of $E_{t,Li} = (190 \pm 5)$ meV and $E_{t,o-exc} = (409 \pm 38)$ meV, and apparent hole capture cross sections of $\sigma_{p,Li} = (6.5 \pm 1.6)\times10^{-17}$ cm^2 and $\sigma_{p,o-exc} = (2.3 \pm 0.9)\times10^{-15}$ cm^2 could be extracted, respectively (values given are averages over all measured diodes, and error includes statistical variation). The determined trap energies fall within the range of the ones given in Table I for the (0/−) charge transition levels of the major acceptors, Li_{Ni} and V_{Ni}.

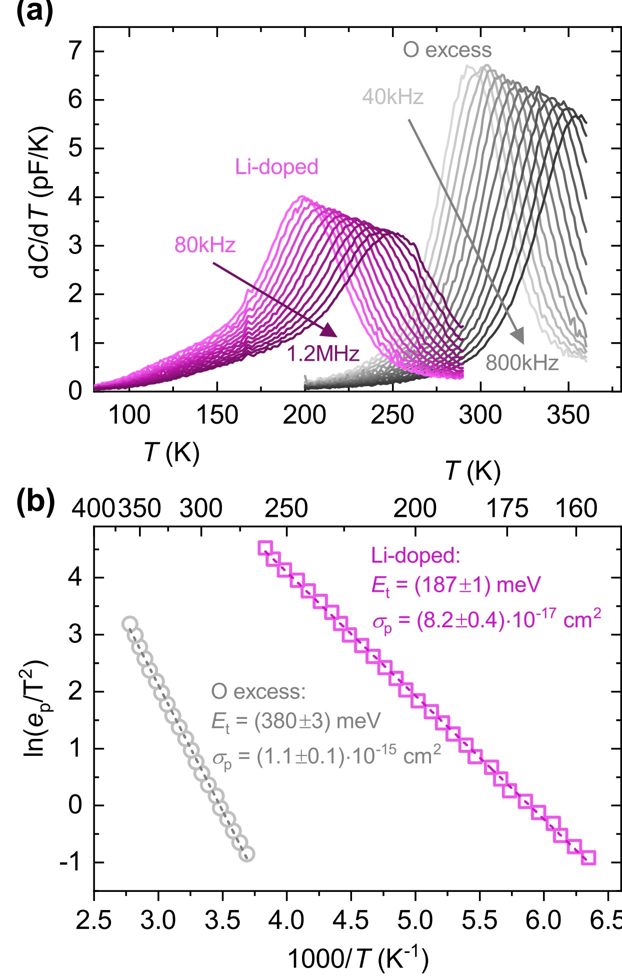

FIG. 3. Thermal admittance spectroscopy results for selected NiO/FTO diodes on oxygen-excess grown and Li-doped NiO films. (a) Differential capacitances and (b) extracted emission rates vs temperature, including fits according to the Arrhenius relation [Eq. (4)].

IV. DISCUSSION

It is compelling to assign the features observed in TAS to ionization processes of the prominent acceptors, and as we will show in the following, this is likely correct. There are, however, two caveats to be discussed. First, being an AC measurement, TAS is capable of detecting processes that critically limit the frequency of the charge transport processes to, from, and around the defects. In conventional semiconductors possessing high free carrier mobilities, carrier capture and emission from traps are the limiting processes in that regard. However, for a low-mobility material like NiO, this assumption should be critically reviewed. It was recently shown[22,24] that the electronic transport in both Li-doped and Ni-deficient NiO can be modeled using a theoretical framework in which the charge carriers form polarons on the acceptor sites and move through the crystal by hopping between closely spaced acceptors (polaronic interacceptor

© Author(s) 2020

hopping, PIH). This process was shown to determine the DC conductivity of an undepleted, doped NiO film to a large extent. The question therefore is if the charge transfer observed by means of TAS in the present paper can be identified with the direct movement of carriers between acceptors, instead of excitation to the valence band and subsequent free carrier movement within that band.

In such a case, the determined activation energy of the trap-like feature should be identical to that for DC transport in undepleted devices. To verify this, we measured the activation energy of an undepleted, Li-doped NiO film, sandwiched between two Pt electrodes, similar to the method described in Ref. 22. σ_{dc} turned out to follow an Arrhenius behavior with an activation energy of approximately 370 meV (see Fig. S2 of the supplementary material). In the framework of the PIH transport model, this energy corresponds to the hopping barrier between two neighboring Li_{Ni} acceptors. Using the data from Ref. 24 as reference, an intersite separation larger than 4 nm, or a Li_{Ni} concentration of below 0.03 at. %, can be inferred. This agrees well with the net doping measured on our films. The process observed by TAS on an identically fabricated, but depleted, Li-doped NiO layer possessing an activation energy of 190 meV, as in Fig. 3(b), can therefore not be related to the cutoff of the intersite hopping transport. For the sample grown under O excess conditions, the activation energies for the TAS peak and the DC conductivity, the latter being around 380 meV as determined in Ref. 22, are very similar. However, a key ingredient of the PIH transport model is the critical dependence of the hopping barrier height on the intersite separation. Although being more stable thermally than the room temperature grown NiO films discussed in Ref. 25, even the O excess sample grown at elevated temperatures in this work exhibited a slow decrease of V_{Ni} acceptor density with time. After the sample had been stored at room temperature for about 18 months, renewed measurements revealed that the net doping of the film had decreased by a factor of 20, from 1.4×10^{18} cm^{-3} to 7×10^{16} cm^{-3} (inset in Fig. S3 of the supplementary material). This is even lower than the net doping of the intentionally annealed, room temperature grown samples studied in Ref. 25. It is therefore reasonable to assume that the intersite hopping barrier in the long-time room temperature-annealed film investigated in this work is at least as large as in the referenced samples, i.e., 700 meV–800 meV. However, renewed TAS measurements on the same, but aged, HT-grown sample revealed that the rates associated with the TAS peak had not changed (Fig. S3 in the supplementary material). For that reason, it can be concluded that also in the O excess sample, the TAS feature is unrelated to a frequency cutoff of the PIH transport process.

To understand why interacceptor transport does not play any role in the AC capacitance signal of the depleted devices, it is insightful to consider what conditions would have to be met in order for an acceptor state to be ionized through intersite hopping alone. An increase in space charge only occurs when the total concentration of holes bound to the acceptors decreases, i.e., holes leave the NiO layer by interacceptor hopping until they reach the Pt back contact. This means that the carrier has to travel over a distance of the order of 100 nm (from inside the space charge region to the NiO/Pt interface). Since this region is mainly field-free, the carrier movement would be diffusion-limited. Assuming an effective mobility for interacceptor hopping of the order of 2×10^{-7} cm^2 V^{-1} s^{-1} in line with Ref. 22, and based on the Einstein relation $D = \mu k_B T/e$, the hole diffusivity at room temperature is roughly $D = 5 \times 10^{-9}$ cm^2 s^{-1}. The hole transit through the entire quasi-neutral region of length $l_{qn} \approx 100$ nm therefore takes about $t_{diff} = l_{qn}^2/D = 20$ ms, which is equivalent to a carrier removal rate through PIH of the order of 50 s^{-1}. This is considerably lower than the measured emission rates. In other words, PIH does not offer hopping rates high enough to extract a significant amount of holes within one measurement cycle, compared to hole excitation from the trap to the valence band and extraction therein.

The next issue possibly arising when carriers are excited into the valence band is posed by low mobility within that band. In a recent publication, Wang *et al.* explored the implications of low carrier mobility (i.e., hopping transport even in the extended states of the host crystal) on TAS spectra by means of numerical simulations.[28] The authors conclude that in such materials, a frequency cutoff originating from carrier mobility freeze-out, a so-called dielectric relaxation peak (DRP), may occur within the studied frequency range. Such a feature may be mistaken for a defect signature, and it may also superimpose other features that actually are related to a defect response if the hopping rate in the band is lower than the escape frequency from an acceptor. It has been speculated early on that the *d* electronic character of valence band states in NiO leads to localization of holes, and transport was suggested to be due to a hopping mechanism even in band-like extended states.[20] Consequently, also the transport within the valence band may be via hopping. Therefore, the possibility of the occurrence of dielectric relaxation in TAS measurements needs to be critically reviewed.

Wang *et al.* found a DRP to dominate the TAS spectrum of a heterostructure comprising the organic semiconductor P3HT.[28] The work by Reislöhner, Metzner, and Ronning revealed that the freeze-out of the mobility of hopping carriers in Cu(In,Ga)Se_2 layers produces a trap-like feature.[29] If the features observed by TAS in this work were caused by the freeze-out of hopping transport in the bands, the critical temperature would be independent of the acceptor type. This is in clear contrast to what is observed in Fig. 3(a): comparing the Li-doped and the O excess sample, the peak temperatures differ by about 100 K for the same set of measurement frequencies. Such a strong dopant dependency is incompatible with the assumption of a cutoff of hopping transport in the bands within the frequency and temperature window used here. Therefore, the observed features in TAS are not caused by a dielectric relaxation.

Based on these points, we suggest the attribution of the traps detected by TAS to the (0/−) charge transition levels of both the Li_{Ni} and V_{Ni} acceptors. The energy level scheme is shown in Fig. 4, which also includes the literature values from Table I for comparison. We would like to note that in our previous publication,[22] we had tentatively drawn an energy scheme of the V_{Ni} acceptor position with respect to the valence band (Fig. 8 in that reference) in which the acceptor level was estimated to be situated more than 1 eV above the valence band. That estimation was based on optical absorption data of highly doped NiO films that typically display a strong absorption band in the near infrared spectral region (at 1.2 eV for Li doping[30] and around 1.5 eV for doping via V_{Ni}[31]). The now experimentally determined, and considerably lower, values of the thermal ionization energies of the acceptors lead to a correction of that picture, thereby underlining the strong polaronic character of charge carriers bound to acceptors in NiO.

© Author(s) 2020

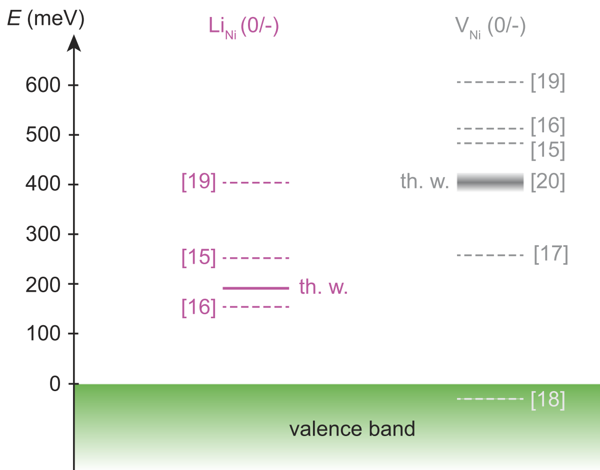

FIG. 4. Energy level scheme of the Li_{Ni} and V_{Ni} (0/−) charge transition levels as determined in this work, along with values from the literature.

It is also interesting to note the large difference in the values obtained for the apparent hole capture cross sections of the acceptors (6.5×10^{-17} cm^2 for the Li_{Ni} and 2.3×10^{-15} cm^2 for the V_{Ni} acceptor, respectively). This may point toward fundamental differences in trap properties, such as the spatial extension of the trap electrostatic potential. As vacancies tend to locally deform the lattice to a larger extent than a substitutional ion with well-matched ion radius, like Li in NiO, one can expect the vacancy to create stronger local strain that could also extend the range of electrostatic forces in the vicinity of the trap.

A second ionization of V_{Ni}, the (−/2−) CTL, has not been observed within our experiments. Since the value for the (0/−) CTL from Ref. 21 matches our experimental one well, we use the value for the (−/2−) level of 600 meV given in that reference to estimate the temperature window for an observation of the second ionization, assuming that the hole capture cross section is identical to that of the (0/−) CTL. For the same set of frequencies shown in Fig. 3(a), the temperature window where the (−/2−) CTL of V_{Ni} can be expected to be observed in TAS is 435 K–525 K.

V. CONCLUSION

We have studied SnO_2:F/NiO $n^{++}p$ heterostructures with Li-doped or O-rich NiO films, respectively. These structures are current-rectifying with a rectification ratio between one and two orders of magnitude at ±1 V, indicating a depletion layer within the NiO. This structure enabled the characterization of trap levels by means of space charge spectroscopy. Using thermal admittance spectroscopy, we have found one dominant feature that can clearly be attributed to hole capture to and emission from one trap level per doping type. We tentatively attribute these levels to the (0/−) charge transition levels of the two prominent acceptors Li_{Ni} and V_{Ni}, which are found at (190 ± 5) meV and (409 ± 38) eV above the valence band edge, in compliance with literature values. The apparent hole capture cross sections of the traps have been determined to be (6.5 ± 1.6) $\times 10^{-17}$ cm^2 for the Li_{Ni} and (2.3 ± 0.9) $\times 10^{-15}$ cm^2 for the V_{Ni} acceptor, respectively.

SUPPLEMENTARY MATERIAL

The supplementary material contains structural data of a Li-doped NiO film grown on FTO obtained from x-ray diffraction, data on the temperature dependence of the DC electric conductivity of undepleted Li-doped NiO, and TAS measurements on as-deposited and aged O excess NiO films.

ACKNOWLEDGMENTS

This work was funded by the Deutsche Forschungsgemeinschaft (DFG, German Research Foundation)—Project No. 31047526, SFB762, Project No. B06. Financial support was kindly provided by the Research Council of Norway and the University of Oslo through the frontier research project FUNDAMeNT (No. 251131, FriProToppForsk-program). The Research Council of Norway is acknowledged for the support to the Norwegian Micro- and Nano-Fabrication Facility, NorFab, Project No. 245963.

DATA AVAILABILITY

The data that support the findings of this study are available from the corresponding author upon reasonable request.

REFERENCES

[1] J. He, H. Lindström, A. Hagfeldt, and S.-E. Lindquist, "Dye-sensitized nanostructured p-type nickel oxide film as a photocathode for a solar cell," J. Phys. Chem. B **103**, 8940–8943 (1999).
[2] M. D. Irwin, D. B. Buchholz, A. W. Hains, R. P. H. Chang, and T. J. Marks, "p-Type semiconducting nickel oxide as an efficiency-enhancing anode interfacial layer in polymer bulk-heterojunction solar cells," Proc. Natl. Acad. Sci. U. S. A. **105**, 2783–2787 (2008).
[3] S.-Y. Park, H.-R. Kim, Y.-J. Kang, D.-H. Kim, and J.-W. Kang, "Organic solar cells employing magnetron sputtered p-type nickel oxide thin film as the anode buffer layer," Sol. Energy Mater. Sol. Cells **94**, 2332–2336 (2010).
[4] J.-Y. Jeng, K.-C. Chen, T.-Y. Chiang, P.-Y. Lin, T.-D. Tsai, Y.-C. Chang, T.-F. Guo, P. Chen, T.-C. Wen, and Y.-J. Hsu, "Nickel oxide electrode interlayer in $CH_3NH_3PbI_3$ Perovskite/PCBM planar-heterojunction hybrid solar cells," Adv. Mater. **26**, 4107–4113 (2014).
[5] S.-W. Park, J.-M. Choi, E. Kim, and S. Im, "Inverted top-emitting organic light-emitting diodes using transparent conductive NiO electrode," Appl. Surf. Sci. **244**, 439–443 (2005).
[6] L. Y. Tang, X. L. Zhang, H. T. Dai, J. L. Zhao, S. G. Wang, and X. W. Sun, "NiO as hole transport layers for all-inorganic quantum dot LEDs," in *Light-Emitting Diodes: Materials, Devices, and Applications for Solid State Lighting XVII*, edited by K. P. Streubel, H. Jeon, L.-W. Tu, and M. Strassburg (SPIE, 2013).
[7] E. Avendaño, L. Berggren, G. A. Niklasson, C. G. Granqvist, and A. Azens, "Electrochromic materials and devices: Brief survey and new data on optical absorption in tungsten oxide and nickel oxide films," Thin Solid Films **496**, 30–36 (2006).
[8] H. Huang, J. Tian, W. K. Zhang, Y. P. Gan, X. Y. Tao, X. H. Xia, and J. P. Tu, "Electrochromic properties of porous NiO thin film as a counter electrode for NiO/WO_3 complementary electrochromic window," Electrochim. Acta **56**, 4281–4286 (2011).
[9] H. Moulki, D. H. Park, B.-K. Min, H. Kwon, S.-J. Hwang, J.-H. Choy, T. Toupance, G. Campet, and A. Rougier, "Improved electrochromic performances of NiO based thin films by lithium addition: From single layers to devices," Electrochim. Acta **74**, 46–52 (2012).

© Author(s) 2020

[10]Y. Ren, W. K. Chim, L. Guo, H. Tanoto, J. Pan, and S. Y. Chiam, "The coloration and degradation mechanisms of electrochromic nickel oxide," Sol. Energy Mater. Sol. Cells **116**, 83–88 (2013).

[11]S. Seo, M. J. Lee, D. C. Kim, S. E. Ahn, B.-H. Park, Y. S. Kim, I. K. Yoo, I. S. Byun, I. R. Hwang, S. H. Kim, J.-S. Kim, J. S. Choi, J. H. Lee, S. H. Jeon, S. H. Hong, and B. H. Park, "Electrode dependence of resistance switching in polycrystalline NiO films," Appl. Phys. Lett. **87**, 263507 (2005).

[12]S. I. Kim, J. H. Lee, Y. W. Chang, S. S. Hwang, and K.-H. Yoo, "Reversible resistive switching behaviors in NiO nanowires," Appl. Phys. Lett. **93**, 033503 (2008).

[13]P. Kuiper, G. Kruizinga, J. Ghijsen, G. A. Sawatzky, and H. Verweij, "Character of holes in $Li_xNi_{1-x}O$ and their magnetic behavior," Phys. Rev. Lett. **62**, 221–224 (1989).

[14]R. J. O. Mossanek, G. Domínguez-Cañizares, A. Gutiérrez, M. Abbate, D. Díaz-Fernández, and L. Soriano, "Effects of Ni vacancies and crystallite size on the O 1s and Ni 2p x-ray absorption spectra of nanocrystalline NiO," J. Phys.: Condens. Matter **25**, 495506 (2013).

[15]H. Wu and L.-S. Wang, "A study of nickel monoxide (NiO), nickel dioxide (ONiO), and $Ni(O_2)$ complex by anion photoelectron spectroscopy," J. Chem. Phys. **107**, 16–21 (1997).

[16]S. Lany, J. Osorio-Guillén, and A. Zunger, "Origins of the doping asymmetry in oxides: Hole doping in NiO versus electron doping in ZnO," Phys. Rev. B **75**, 241203 (2007).

[17]P. Wu, V. Ligatchev, Z. G. Yu, J. Zheng, M. B. Sullivan, and Y. Zeng, "Defects in codoped NiO with gigantic dielectric response," Phys. Rev. B **79**, 235122 (2009).

[18]W.-B. Zhang, N. Yu, W.-Y. Yu, and B.-Y. Tang, "Stability and magnetism of vacancy in NiO: A GGA+U study," Eur. Phys. J. B **64**, 153–158 (2008).

[19]H. D. Lee, B. Magyari-Köpe, and Y. Nishi, "Model of metallic filament formation and rupture in NiO for unipolar switching," Phys. Rev. B **81**, 193202 (2010).

[20]D. Adler and J. Feinleib, "Electrical and optical properties of narrow-band materials," Phys. Rev. B **2**, 3112–3134 (1970).

[21]J. A. Dawson, Y. Guo, and J. Robertson, "Energetics of intrinsic defects in NiO and the consequences for its resistive random access memory performance," Appl. Phys. Lett. **107**, 122110 (2015).

[22]R. Karsthof, M. Grundmann, A. M. Anton, and F. Kremer, "Polaronic inter-acceptor hopping transport in intrinsically doped nickel oxide," Phys. Rev. B **99**, 235201 (2019).

[23]V. A. Johnson, R. N. Smith, and H. J. Yearian, "D.C. characteristics of silicon and germanium point contact crystal rectifiers. Part II. The multicontact theory," J. Appl. Phys. **21**, 283–289 (1950).

[24]Y. Kokubun and S. Nakagomi, "Electrical conductivity studies in sol-gel-derived Li-doped NiO epitaxial thin films," Phys. Status Solidi B (published online, 2020).

[25]R. Karsthof, A. M. Anton, F. Kremer, and M. Grundmann, "Nickel vacancy acceptor in nickel oxide: Doping beyond thermodynamic equilibrium," Phys. Rev. Mater. **4**, 034601 (2020).

[26]A. Gutiérrez, G. Domínguez-Cañizares, S. Krause, D. Díaz-Fernández, and L. Soriano, "Thermal induced depletion of cationic vacancies in NiO thin films evidenced by x-ray absorption spectroscopy at the O 1s threshold," J. Vac. Sci. Technol. A **38**, 033209 (2020).

[27]T. Walter, R. Herberholz, C. Müller, and H. W. Schock, "Determination of defect distributions from admittance measurements and application to $Cu(In,Ga)Se_2$ based heterojunctions," J. Appl. Phys. **80**, 4411–4420 (1996).

[28]S. Wang, P. Kaienburg, B. Klingebiel, D. Schillings, and T. Kirchartz, "Understanding thermal admittance spectroscopy in low-mobility semiconductors," J. Phys. Chem. C **122**, 9795–9803 (2018).

[29]U. Reislöhner, H. Metzner, and C. Ronning, "Hopping conduction observed in thermal admittance spectroscopy," Phys. Rev. Lett. **104**, 226403 (2010).

[30]J. Y. Zhang, W. W. Li, R. L. Z. Hoye, J. L. MacManus-Driscoll, M. Budde, O. Bierwagen, L. Wang, Y. Du, M. J. Wahila, L. F. J. Piper, T.-L. Lee, H. J. Edwards, V. R. Dhanak, and K. H. L. Zhang, "Electronic and transport properties of Li-doped NiO epitaxial thin films," J. Mater. Chem. C **6**, 2275–2282 (2018).

[31]K. O. Egbo, C. P. Liu, C. E. Ekuma, and K. M. Yu, "Vacancy defects induced changes in the electronic and optical properties of NiO studied by spectroscopic ellipsometry and first-principles calculations," J. Appl. Phys. **128**, 135705 (2020).

© Author(s) 2020